Search for direct CP violation in singly Cabibbo-suppressed $D^{\pm} \to K^+K^-\pi^{\pm}$ decays

J. P. Lees,[1] V. Poireau,[1] V. Tisserand,[1] J. Garra Tico,[2] E. Grauges,[2] A. Palano,[3a,3b] G. Eigen,[4] B. Stugu,[4] D. N. Brown,[5] L. T. Kerth,[5] Yu. G. Kolomensky,[5] G. Lynch,[5] H. Koch,[6] T. Schroeder,[6] D. J. Asgeirsson,[7] C. Hearty,[7] T. S. Mattison,[7] J. A. McKenna,[7] R. Y. So,[7] A. Khan,[8] V. E. Blinov,[9] A. R. Buzykaev,[9] V. P. Druzhinin,[9] V. B. Golubev,[9] E. A. Kravchenko,[9] A. P. Onuchin,[9] S. I. Serednyakov,[9] Yu. I. Skovpen,[9] E. P. Solodov,[9] K. Yu. Todyshev,[9] A. N. Yushkov,[9] M. Bondioli,[10] D. Kirkby,[10] A. J. Lankford,[10] M. Mandelkern,[10] H. Atmacan,[11] J. W. Gary,[11] F. Liu,[11] O. Long,[11] G. M. Vitug,[11] C. Campagnari,[12] T. M. Hong,[12] D. Kovalskyi,[12] J. D. Richman,[12] C. A. West,[12] A. M. Eisner,[13] J. Kroseberg,[13] W. S. Lockman,[13] A. J. Martinez,[13] B. A. Schumm,[13] A. Seiden,[13] D. S. Chao,[14] C. H. Cheng,[14] B. Echenard,[14] K. T. Flood,[14] D. G. Hitlin,[14] P. Ongmongkolkul,[14] F. C. Porter,[14] A. Y. Rakitin,[14] R. Andreassen,[15] Z. Huard,[15] B. T. Meadows,[15] M. D. Sokoloff,[15] L. Sun,[15] P. C. Bloom,[16] W. T. Ford,[16] A. Gaz,[16] U. Nauenberg,[16] J. G. Smith,[16] S. R. Wagner,[16] R. Ayad,[17,*] W. H. Toki,[17] B. Spaan,[18] K. R. Schubert,[19] R. Schwierz,[19] D. Bernard,[20] M. Verderi,[20] P. J. Clark,[21] S. Playfer,[21] D. Bettoni,[22a] C. Bozzi,[22a] R. Calabrese,[22a,22b] G. Cibinetto,[22a,22b] E. Fioravanti,[22a,22b] I. Garzia,[22a,22b] E. Luppi,[22a,22b] L. Piemontese,[22a] V. Santoro,[22a] R. Baldini-Ferroli,[23] A. Calcaterra,[23] R. de Sangro,[23] G. Finocchiaro,[23] P. Patteri,[23] I. M. Peruzzi,[23,†] M. Piccolo,[23] M. Rama,[23] A. Zallo,[23] R. Contri,[24a,24b] E. Guido,[24a,24b] M. Lo Vetere,[24a,24b] M. R. Monge,[24a,24b] S. Passaggio,[24a] C. Patrignani,[24a,24b] E. Robutti,[24a] B. Bhuyan,[25] V. Prasad,[25] C. L. Lee,[26] M. Morii,[26] A. J. Edwards,[27] A. Adametz,[28] U. Uwer,[28] H. M. Lacker,[29] T. Lueck,[29] P. D. Dauncey,[30] U. Mallik,[31] C. Chen,[32] J. Cochran,[32] W. T. Meyer,[32] S. Prell,[32] A. E. Rubin,[32] A. V. Gritsan,[33] Z. J. Guo,[33] N. Arnaud,[34] M. Davier,[34] D. Derkach,[34] G. Grosdidier,[34] F. Le Diberder,[34] A. M. Lutz,[34] B. Malaescu,[34] P. Roudeau,[34] M. H. Schune,[34] A. Stocchi,[34] G. Wormser,[34] D. J. Lange,[35] D. M. Wright,[35] C. A. Chavez,[36] J. P. Coleman,[36] J. R. Fry,[36] E. Gabathuler,[36] D. E. Hutchcroft,[36] D. J. Payne,[36] C. Touramanis,[36] A. J. Bevan,[37] F. Di Lodovico,[37] R. Sacco,[37] M. Sigamani,[37] G. Cowan,[38] D. N. Brown,[39] C. L. Davis,[39] A. G. Denig,[40] M. Fritsch,[40] W. Gradl,[40] K. Griessinger,[40] A. Hafner,[40] E. Prencipe,[40] R. J. Barlow,[41,‡] G. Jackson,[41] G. D. Lafferty,[41] E. Behn,[42] R. Cenci,[42] B. Hamilton,[42] A. Jawahery,[42] D. A. Roberts,[42] C. Dallapiccola,[43] R. Cowan,[44] D. Dujmic,[44] G. Sciolla,[44] R. Cheaib,[45] D. Lindemann,[45] P. M. Patel,[45,§] S. H. Robertson,[45] P. Biassoni,[46a,46b] N. Neri,[46a] F. Palombo,[46a,46b] S. Stracka,[46a,46b] L. Cremaldi,[47] R. Godang,[47,‖] R. Kroeger,[47] P. Sonnek,[47] D. J. Summers,[47] X. Nguyen,[48] M. Simard,[48] P. Taras,[48] G. De Nardo,[49a,49b] D. Monorchio,[49a,49b] G. Onorato,[49a,49b] C. Sciacca,[49a,49b] M. Martinelli,[50] G. Raven,[50] C. P. Jessop,[51] J. M. LoSecco,[51] W. F. Wang,[51] K. Honscheid,[52] R. Kass,[52] J. Brau,[53] R. Frey,[53] N. B. Sinev,[53] D. Strom,[53] E. Torrence,[53] E. Feltresi,[54a,54b] N. Gagliardi,[54a,54b] M. Margoni,[54a,54b] M. Morandin,[54a] M. Posocco,[54a] M. Rotondo,[54a] G. Simi,[54a] F. Simonetto,[54a,54b] R. Stroili,[54a,54b] S. Akar,[55] E. Ben-Haim,[55] M. Bomben,[55] G. R. Bonneaud,[55] H. Briand,[55] G. Calderini,[55] J. Chauveau,[55] O. Hamon,[55] Ph. Leruste,[55] G. Marchiori,[55] J. Ocariz,[55] S. Sitt,[55] M. Biasini,[56a,56b] E. Manoni,[56a,56b] S. Pacetti,[56a,56b] A. Rossi,[56a,56b] C. Angelini,[57a,57b] G. Batignani,[57a,57b] S. Bettarini,[57a,57b] M. Carpinelli,[57a,57b,¶] G. Casarosa,[57a,57b] A. Cervelli,[57a,57b] F. Forti,[57a,57b] M. A. Giorgi,[57a,57b] A. Lusiani,[57a,57c] B. Oberhof,[57a,57b] E. Paoloni,[57a,57b] A. Perez,[57a] G. Rizzo,[57a,57b] J. J. Walsh,[57a] D. Lopes Pegna,[58] J. Olsen,[58] A. J. S. Smith,[58] A. V. Telnov,[58] F. Anulli,[59a] R. Faccini,[59a,59b] F. Ferrarotto,[59a] F. Ferroni,[59a,59b] M. Gaspero,[59a,59b] L. Li Gioi,[59a] M. A. Mazzoni,[59a] G. Piredda,[59a] C. Bünger,[60] O. Grünberg,[60] T. Hartmann,[60] T. Leddig,[60] C. Voß,[60] R. Waldi,[60] T. Adye,[61] E. O. Olaiya,[61] F. F. Wilson,[61] S. Emery,[62] G. Hamel de Monchenault,[62] G. Vasseur,[62] Ch. Yèche,[62] D. Aston,[63] D. J. Bard,[63] R. Bartoldus,[63] J. F. Benitez,[63] C. Cartaro,[63] M. R. Convery,[63] J. Dorfan,[63] G. P. Dubois-Felsmann,[63] W. Dunwoodie,[63] M. Ebert,[63] R. C. Field,[63] M. Franco Sevilla,[63] B. G. Fulsom,[63] A. M. Gabareen,[63] M. T. Graham,[63] P. Grenier,[63] C. Hast,[63] W. R. Innes,[63] M. H. Kelsey,[63] P. Kim,[63] M. L. Kocian,[63] D. W. G. S. Leith,[63] P. Lewis,[63] B. Lindquist,[63] S. Luitz,[63] V. Luth,[63] H. L. Lynch,[63] D. B. MacFarlane,[63] D. R. Muller,[63] H. Neal,[63] S. Nelson,[63] M. Perl,[63] T. Pulliam,[63] B. N. Ratcliff,[63] A. Roodman,[63] A. A. Salnikov,[63] R. H. Schindler,[63] A. Snyder,[63] D. Su,[63] M. K. Sullivan,[63] J. Va'vra,[63] A. P. Wagner,[63] W. J. Wisniewski,[63] M. Wittgen,[63] D. H. Wright,[63] H. W. Wulsin,[63] C. C. Young,[63] V. Ziegler,[63] W. Park,[64] M. V. Purohit,[64] R. M. White,[64] J. R. Wilson,[64] A. Randle-Conde,[65] S. J. Sekula,[65] M. Bellis,[66] P. R. Burchat,[66] T. S. Miyashita,[66] E. M. T. Puccio,[66] M. S. Alam,[67] J. A. Ernst,[67] R. Gorodeisky,[68] N. Guttman,[68] D. R. Peimer,[68] A. Soffer,[68] P. Lund,[69] S. M. Spanier,[69] J. L. Ritchie,[70] A. M. Ruland,[70] R. F. Schwitters,[70] B. C. Wray,[70] J. M. Izen,[71] X. C. Lou,[71] F. Bianchi,[72a,72b] D. Gamba,[72a,72b] S. Zambito,[72a,72b] L. Lanceri,[73a,73b] L. Vitale,[73a,73b] F. Martinez-Vidal,[74] A. Oyanguren,[74] P. Villanueva-Perez,[74] H. Ahmed,[75] J. Albert,[75] Sw. Banerjee,[75] F. U. Bernlochner,[75] H. H. F. Choi,[75] G. J. King,[75] R. Kowalewski,[75] M. J. Lewczuk,[75] I. M. Nugent,[75] J. M. Roney,[75] R. J. Sobie,[75] N. Tasneem,[75] T. J. Gershon,[76] P. F. Harrison,[76] T. E. Latham,[76] H. R. Band,[77] S. Dasu,[77] Y. Pan,[77] R. Prepost,[77] and S. L. Wu[77]

(*BABAR* Collaboration)

[1]*Laboratoire d'Annecy-le-Vieux de Physique des Particules (LAPP), Université de Savoie, CNRS/IN2P3, F-74941 Annecy-Le-Vieux, France*
[2]*Departament ECM, Facultat de Fisica, Universitat de Barcelona, E-08028 Barcelona, Spain*
[3a]*INFN Sezione di Bari, I-70126 Bari, Italy*
[3b]*Dipartimento di Fisica, Università di Bari, I-70126 Bari, Italy*
[4]*Institute of Physics, University of Bergen, N-5007 Bergen, Norway*
[5]*Lawrence Berkeley National Laboratory and University of California, Berkeley, California 94720, USA*
[6]*Institut für Experimentalphysik 1, Ruhr Universität Bochum, D-44780 Bochum, Germany*
[7]*University of British Columbia, Vancouver, British Columbia, Canada V6T 1Z1*
[8]*Brunel University, Uxbridge, Middlesex UB8 3PH, United Kingdom*
[9]*Budker Institute of Nuclear Physics, Novosibirsk 630090, Russia*
[10]*University of California at Irvine, Irvine, California 92697, USA*
[11]*University of California at Riverside, Riverside, California 92521, USA*
[12]*University of California at Santa Barbara, Santa Barbara, California 93106, USA*
[13]*Institute for Particle Physics, University of California at Santa Cruz, Santa Cruz, California 95064, USA*
[14]*California Institute of Technology, Pasadena, California 91125, USA*
[15]*University of Cincinnati, Cincinnati, Ohio 45221, USA*
[16]*University of Colorado, Boulder, Colorado 80309, USA*
[17]*Colorado State University, Fort Collins, Colorado 80523, USA*
[18]*Fakultät Physik, Technische Universität Dortmund, D-44221 Dortmund, Germany*
[19]*Institut für Kern- und Teilchenphysik, Technische Universität Dresden, D-01062 Dresden, Germany*
[20]*Laboratoire Leprince-Ringuet, Ecole Polytechnique, CNRS/IN2P3, F-91128 Palaiseau, France*
[21]*University of Edinburgh, Edinburgh EH9 3JZ, United Kingdom*
[22a]*INFN Sezione di Ferrara, I-44100 Ferrara, Italy*
[22b]*Dipartimento di Fisica, Università di Ferrara, I-44100 Ferrara, Italy*
[23]*INFN Laboratori Nazionali di Frascati, I-00044 Frascati, Italy*
[24a]*INFN Sezione di Genova, I-16146 Genova, Italy*
[24b]*Dipartimento di Fisica, Università di Genova, I-16146 Genova, Italy*
[25]*Indian Institute of Technology Guwahati, Guwahati, Assam 781039, India*
[26]*Harvard University, Cambridge, Massachusetts 02138, USA*
[27]*Harvey Mudd College, Claremont, California 91711, USA*
[28]*Physikalisches Institut, Universität Heidelberg, Philosophenweg 12, D-69120 Heidelberg, Germany*
[29]*Institut für Physik, Humboldt-Universität zu Berlin, Newtonstrasse 15, D-12489 Berlin, Germany*
[30]*Imperial College London, London SW7 2AZ, United Kingdom*
[31]*University of Iowa, Iowa City, Iowa 52242, USA*
[32]*Iowa State University, Ames, Iowa 50011-3160, USA*
[33]*Johns Hopkins University, Baltimore, Maryland 21218, USA*
[34]*Laboratoire de l'Accélérateur Linéaire, IN2P3/CNRS et Université Paris-Sud 11, Centre Scientifique d'Orsay, B. P. 34, F-91898 Orsay Cedex, France*
[35]*Lawrence Livermore National Laboratory, Livermore, California 94550, USA*
[36]*University of Liverpool, Liverpool L69 7ZE, United Kingdom*
[37]*Queen Mary, University of London, London E1 4NS, United Kingdom*
[38]*Royal Holloway and Bedford New College, University of London, Egham, Surrey TW20 0EX, United Kingdom*
[39]*University of Louisville, Louisville, Kentucky 40292, USA*
[40]*Institut für Kernphysik, Johannes Gutenberg-Universität Mainz, D-55099 Mainz, Germany*
[41]*University of Manchester, Manchester M13 9PL, United Kingdom*
[42]*University of Maryland, College Park, Maryland 20742, USA*
[43]*University of Massachusetts, Amherst, Massachusetts 01003, USA*
[44]*Laboratory for Nuclear Science, Massachusetts Institute of Technology, Cambridge, Massachusetts 02139, USA*
[45]*McGill University, Montréal, Québec, Canada H3A 2T8*
[46a]*INFN Sezione di Milano, I-20133 Milano, Italy*
[46b]*Dipartimento di Fisica, Università di Milano, I-20133 Milano, Italy*
[47]*University of Mississippi, University, Mississippi 38677, USA*
[48]*Physique des Particules, Université de Montréal, Montréal, Québec, Canada H3C 3J7*
[49a]*INFN Sezione di Napoli, I-80126 Napoli, Italy*
[49b]*Dipartimento di Scienze Fisiche, Università di Napoli Federico II, I-80126 Napoli, Italy*
[50]*NIKHEF, National Institute for Nuclear Physics and High Energy Physics, NL-1009 DB Amsterdam, The Netherlands*

[51]*University of Notre Dame, Notre Dame, Indiana 46556, USA*
[52]*Ohio State University, Columbus, Ohio 43210, USA*
[53]*University of Oregon, Eugene, Oregon 97403, USA*
[54a]*INFN Sezione di Padova, I-35131 Padova, Italy*
[54b]*Dipartimento di Fisica, Università di Padova, I-35131 Padova, Italy*
[55]*Laboratoire de Physique Nucléaire et de Hautes Energies, IN2P3/CNRS, Université Pierre et Marie Curie-Paris6, Université Denis Diderot-Paris7, F-75252 Paris, France*
[56a]*INFN Sezione di Perugia, I-06100 Perugia, Italy*
[56b]*Dipartimento di Fisica, Università di Perugia, I-06100 Perugia, Italy*
[57a]*INFN Sezione di Pisa, I-56127 Pisa, Italy*
[57b]*Dipartimento di Fisica, Università di Pisa, I-56127 Pisa, Italy*
[57c]*Scuola Normale Superiore di Pisa, I-56127 Pisa, Italy*
[58]*Princeton University, Princeton, New Jersey 08544, USA*
[59a]*INFN Sezione di Roma, I-00185 Roma, Italy*
[59b]*Dipartimento di Fisica, Università di Roma La Sapienza, I-00185 Roma, Italy*
[60]*Universität Rostock, D-18051 Rostock, Germany*
[61]*Rutherford Appleton Laboratory, Chilton, Didcot, Oxon OX11 0QX, United Kingdom*
[62]*CEA, Irfu, SPP, Centre de Saclay, F-91191 Gif-sur-Yvette, France*
[63]*SLAC National Accelerator Laboratory, Stanford, California 94309, USA*
[64]*University of South Carolina, Columbia, South Carolina 29208, USA*
[65]*Southern Methodist University, Dallas, Texas 75275, USA*
[66]*Stanford University, Stanford, California 94305-4060, USA*
[67]*State University of New York, Albany, New York 12222, USA*
[68]*School of Physics and Astronomy, Tel Aviv University, Tel Aviv 69978, Israel*
[69]*University of Tennessee, Knoxville, Tennessee 37996, USA*
[70]*University of Texas at Austin, Austin, Texas 78712, USA*
[71]*University of Texas at Dallas, Richardson, Texas 75083, USA*
[72a]*INFN Sezione di Torino, I-10125 Torino, Italy*
[72b]*Dipartimento di Fisica Sperimentale, Università di Torino, I-10125 Torino, Italy*
[73a]*INFN Sezione di Trieste, I-34127 Trieste, Italy*
[73b]*Dipartimento di Fisica, Università di Trieste, I-34127 Trieste, Italy*
[74]*IFIC, Universitat de Valencia-CSIC, E-46071 Valencia, Spain*
[75]*University of Victoria, Victoria, British Columbia, Canada V8W 3P6*
[76]*Department of Physics, University of Warwick, Coventry CV4 7AL, United Kingdom*
[77]*University of Wisconsin, Madison, Wisconsin 53706, USA*
(Received 11 December 2012; published 6 March 2013)

We report on a search for direct *CP* violation in the singly Cabibbo-suppressed decay $D^+ \to K^+K^-\pi^+$ using a data sample of 476 fb^{-1} of e^+e^- annihilation data accumulated with the *BABAR* detector at the SLAC PEP-II electron-positron collider, running at and just below the energy of the $\Upsilon(4S)$ resonance. The integrated *CP*-violating decay rate asymmetry A_{CP} is determined to be $(0.37 \pm 0.30 \pm 0.15)\%$. Model-independent and model-dependent Dalitz plot analysis techniques are used to search for *CP*-violating asymmetries in the various intermediate states. We find no evidence for *CP*-violation asymmetry.

DOI: 10.1103/PhysRevD.87.052010 PACS numbers: 11.30.Er, 13.25.Ft, 14.40.Lb

I. INTRODUCTION

Searches for *CP* violation (*CPV*) in charm meson decays provide a probe of physics beyond the Standard Model. Singly Cabibbo-suppressed (SCS) decays can exhibit direct *CP* asymmetries due to interference between tree-level transitions and $|\Delta C| = 1$ penguin-level transitions if there is both a strong and a weak phase difference between the two amplitudes. In the Standard Model, the resulting asymmetries are suppressed by $\mathcal{O}(|V_{cb}V_{ub}/V_{cs}V_{us}|) \sim 10^{-3}$, where V_{ij} are elements of the Cabibbo-Kobayashi-Maskawa quark-mixing matrix [1]. A larger measured value of the *CP* asymmetry could be a consequence of the

*Present address: University of Tabuk, Tabuk 71491, Saudi Arabia.
†Also with Dipartimento di Fisica, Università di Perugia, Perugia, Italy.
‡Present address: University of Huddersfield, Huddersfield HD1 3DH, UK.
§Deceased.
‖Present address: University of South Alabama, Mobile, Alabama 36688, USA.
¶Also with Università di Sassari, Sassari, Italy.

enhancement of penguin amplitudes in D meson decays due to final-state interactions [2,3] or of new physics [4,5].

The LHCb and CDF Collaborations recently reported evidence for a nonzero CP asymmetry in the difference of the time-integrated $D^0 \to \pi^+\pi^-$ and $D^0 \to K^+K^-$ decay rates [6,7]. Searches for CPV in other SCS decays with identical transitions $c \to ud\bar{d}$ and $c \to us\bar{s}$ are relevant to an understanding of the origin of CPV [8–10].

We present here a study of the SCS decay $D^+ \to K^+K^-\pi^+$ [11], which is dominated by quasi-two-body decays with resonant intermediate states. This allows us to probe the Dalitz-plot substructure for asymmetries in both the magnitudes and phases of the intermediate states. The results of this study include a measurement of the integrated CP asymmetry, the CP asymmetry in four regions of the Dalitz plot, a comparison of the binned D^+ and D^- Dalitz plots, a comparison of the Legendre polynomial moment distributions for the K^+K^- and $K^-\pi^+$ systems, and a comparison of parametrized fits to the Dalitz plots. Previous measurements by the CLEO-c Collaboration found no evidence for CPV in specific two-body amplitudes or for the integrals over the entire phase space [12]. The LHCb Collaboration also finds no evidence for CPV in a model-independent search [13].

II. THE *BABAR* DETECTOR AND DATA SAMPLE

The analysis is based on a sample of electron-positron annihilation data collected at and just below the energy of the $\Upsilon(4S)$ resonance with the *BABAR* detector at the SLAC PEP-II collider, corresponding to an integrated luminosity of 476 fb^{-1}. The *BABAR* detector is described in detail elsewhere [14]. The following is a brief summary of the detector subsystems important to this analysis. Charged-particle tracks are detected, and their momenta measured, by means of the combination of a 40-layer cylindrical drift chamber (DCH) and a five-layer silicon vertex tracker, both operating within a 1.5-T solenoidal magnetic field. Information from a ring-imaging Cherenkov detector (detector of internally reflected Cherenkov light) and specific energy-loss measurements (dE/dx) in the silicon vertex tracker and DCH are used to identify charged kaon and pion candidates.

For various purposes described below, we use samples of Monte Carlo (MC) simulated events generated using the JETSET [15] program. These events are passed through a detector simulation based on the Geant4 toolkit [16]. Signal MC events refer to $D^+ \to K^+K^-\pi^+$ decays generated using JETSET as well as $D^+ \to K^+K^-\pi^+\gamma$ decays generated using JETSET in combination with the PHOTOS [17] program. In all cases when we simulate particle decays, we include EvtGen [18].

III. EVENT SELECTION AND $D^+ \to K^+K^-\pi^+$ RECONSTRUCTION

The three-body $D^+ \to K^+K^-\pi^+$ decay is reconstructed from events having at least three tracks with net charge $+1$. Two oppositely charged tracks must be consistent with the kaon hypothesis. Other charged tracks are assumed to be pions. To improve particle identification performance, there must be at least one photon in the detector of internally reflected Cherenkov light associated with each track. Contamination from electrons is significantly reduced by means of dE/dx information from the DCH. Pion candidates must have transverse momentum $p_T > 300$ MeV/c. For lower p_T values, tracks are poorly reconstructed. Also, for lower p_T, differences in the nuclear cross sections for positively charged and negatively charged particles can lead to asymmetries. We form the invariant mass of $K^+K^-\pi^+$ candidates and require it to lie within 1.82–1.92 GeV/c^2. The three tracks must originate from a common vertex, and the vertex-constrained fit probability ($P_{\rm vtx}$) must be greater than 0.5%. The momentum in the center-of-mass (CM) frame ($p_{\rm CM}$) of the resulting D candidate must lie within the interval [2.4, 5.0] GeV/c. The lower limit on $p_{\rm CM}$ reduces background from B decays by preferentially selecting $e^+e^- \to c\bar{c}$ events; this has traditionally been the way to reduce combinatoric background due to B decays. To remove background from misidentified $D^{*+} \to D^0\pi^+$ decays, we require $m(K^+K^-\pi^+) - m(K^-\pi^+) - m(\pi^+) > 15$ MeV/c^2, where the pion and kaon masses are set to the nominal values [19]. Finally, for events with multiple $D^\pm$ candidates, the combination with the largest value of $P_{\rm vtx}$ is selected. We perform a separate kinematic fit in which the $D^\pm$ mass is constrained to its nominal value [19]. The result of the fit is used in the Dalitz plot and moments analyses described below.

To aid in the discrimination between signal and background events, we use the joint probability density function (PDF) for $L_{\rm xy}$, the distance between the primary event vertex and the D meson decay vertex in the plane transverse to the beam direction, and $p_{\rm CM}$, to form a likelihood ratio,

$$\mathrm{R}_{\mathcal{L}} = \frac{P_{\rm s}(p_{\rm CM})P_{\rm s}(L_{\rm xy})}{P_{\rm s}(p_{\rm CM})P_{\rm s}(L_{\rm xy}) + P_{\rm b}(p_{\rm CM})P_{\rm b}(L_{\rm xy})}. \quad (1)$$

Since the two variables have little correlation, we construct the two-dimensional PDF as simply the product of their one-dimensional PDFs; these one-dimensional PDFs for signal ($P_{\rm s}$) and background ($P_{\rm b}$) are estimated from data. The background PDFs are determined from events in the D^+ mass sidebands, while those for the signal are estimated from events in the D^+ signal region after background is subtracted using estimates from the sidebands. The signal region is defined by the $m(K^+K^-\pi^+)$ interval 1.86–1.88 GeV/c^2, while the sideband regions are the 1.83–1.84 GeV/c^2 and 1.90–1.91 GeV/c^2 intervals. The selection on $\mathrm{R}_{\mathcal{L}}$ is adjusted to maximize signal significance, and the resulting signal is fairly pure (see Fig. 3 in Sec. VI).

The reconstruction efficiency for D^+ decays is determined from a sample of MC events in which the decay is generated according to phase space (i.e., the Dalitz plot is uniformly populated). To parametrize the selection

efficiency, we use the distribution of reconstructed events as a function of the cosine of the polar angle of the D meson in the CM frame [$\cos(\theta_{\rm CM})$] and the $m^2(K^-\pi^+)$ versus $m^2(K^+K^-)$ Dalitz plot. The selection efficiency is determined as the ratio of $N_{\rm Reco}/N_{\rm Gen}$ in intervals of $\cos(\theta_{\rm CM})$ and separately in intervals of the Dalitz plot, where $N_{\rm Reco}$ is the number of selected events in an interval and $N_{\rm Gen}$ is the number of events generated in the same interval. The binned Dalitz-plot efficiency is parametrized with a feed-forward artificial neural network (ANN) [20] consisting of two hidden layers with three and five nodes. Use of an ANN procedure allows us to adequately model the efficiency near the edges of the Dalitz plots. The ANN efficiency function is tested by creating separate training and validation samples, which are satisfactorily fit by the ANN.

IV. CORRECTIONS TO SIMULATED EVENTS

In order to describe accurately the reconstruction efficiency, we apply corrections to the reconstructed MC events to account for known differences between simulated events and data. The differences arise in the reconstruction asymmetry of charged-pion tracks and in the production model for charm mesons. Differences in kaon particle identification efficiency have a negligible asymmetry effect since the K^+ and K^- are common to D^+ and D^- decays.

To correct the production model used in the simulation, we construct the ratio of the two-dimensional $p_{\rm CM}$ versus $\cos(\theta_{\rm CM})$ PDFs between data and simulation and apply this ratio as a correction to the reconstructed MC events before calculating the efficiency. For this procedure the signal PDF for data is background subtracted, while the signal MC events are weighted by the Dalitz plot amplitude squared, determined from data (see Sec. VIII).

To correct for differences in the reconstruction asymmetry of charged-pion tracks, we use a sample of $e^+e^- \to \tau^+\tau^-$ events in which one τ decays leptonically via $\tau^\pm \to \mu^\pm \nu_\mu \nu_\tau$, while the other τ decays hadronically via $\tau^\mp \to h^\mp h^\mp h^\pm \nu_\tau$. We tag events with a single isolated muon on one side of the event and reconstruct the hadronic τ decay in the opposite hemisphere. We refer to this sample as the "Tau31" sample. We further require two of the three hadrons to have an invariant mass consistent with the rho mass to within 100 MeV/c^2. Due to tracking inefficiencies, tau decays to three tracks are sometimes reconstructed with only two tracks. We use the two-dimensional distributions of $\cos\theta_{\pi\pi}$ and $p_{T_{\pi\pi}}$ (with respect to the beam axis) of the rho-decay pions for two-hadron and three-hadron events to determine the pion inefficiency and asymmetry. We allow for a different efficiency for positive and negative tracks ($\varepsilon_\pm$) by introducing the asymmetry $a(p_{\rm Lab})$ as a function of pion laboratory momentum ($p_{\rm Lab}$),

$$a(p_{\rm Lab}) = \frac{\varepsilon_+(p_{\rm Lab}) - \varepsilon_-(p_{\rm Lab})}{\varepsilon_+(p_{\rm Lab}) + \varepsilon_-(p_{\rm Lab})}. \qquad (2)$$

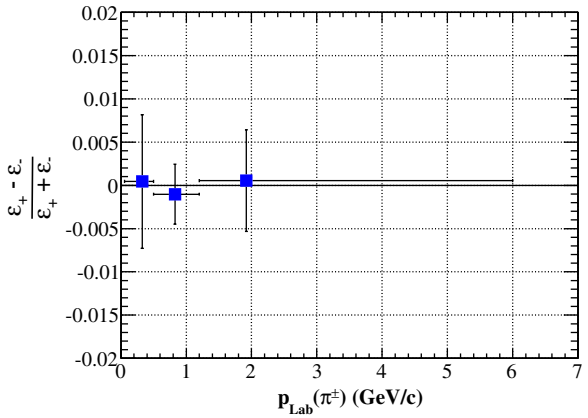

FIG. 1 (color online). Charged pion tracking efficiency asymmetry [defined in Eq. (2)] as a function of the pion momentum in the laboratory frame determined from the decays of τ leptons. The horizontal error bars indicate the range of pion momentum [21].

The results for $a(p_{\rm Lab})$ are shown in Fig. 1: the average value for $0 < p_{\rm Lab} < 4$ GeV/c is $(0.10 \pm 0.26)\%$, which is consistent with zero [21]. We use linear interpolation between data points, or extrapolation beyond the first and last data points, to obtain the ratio of track-efficiency asymmetries between data and MC as a function of momentum. This ratio is then used to correct track efficiencies determined from signal MC.

V. INTEGRATED *CP* ASYMMETRY AS A FUNCTION OF $\cos(\theta_{\rm CM})$

The production of D^+ (and D^-) mesons from the $e^+e^- \to c\bar{c}$ process is not symmetric in $\cos(\theta_{\rm CM})$; this forward-backward (FB) asymmetry, coupled with the asymmetric acceptance of the detector, results in different yields for D^+ and D^- events. The FB asymmetry, to first order, arises from the interference of the separate annihilation processes involving a virtual photon and a Z^0 boson. We define the charge asymmetry A in a given interval of $\cos(\theta_{\rm CM})$ by

$$A(\cos(\theta_{\rm CM})) \equiv \frac{N_{D^+}/\epsilon_{D^+} - N_{D^-}/\epsilon_{D^-}}{N_{D^+}/\epsilon_{D^+} + N_{D^-}/\epsilon_{D^-}}, \qquad (3)$$

where $N_{D^\pm}$ and $\epsilon_{D^\pm}$ are the yield and efficiency, respectively, in the given $\cos(\theta_{\rm CM})$ bin. We remove the FB asymmetry by averaging A over four intervals symmetric in $\cos(\theta_{\rm CM})$, i.e., by evaluating

$$A_{CP} \equiv \frac{A(\cos(\theta_{\rm CM})) + A(-\cos(\theta_{\rm CM}))}{2}. \qquad (4)$$

The interval boundaries in $\cos(\theta_{\rm CM})$ are defined as 0, 0.2, 0.4, 0.6, 1.0. The $D^\pm$ yields are determined from fits to the reconstructed $K^\pm K^\mp \pi^\pm$ mass distributions, as described in Sec. VI. This technique has been used in previous *BABAR* measurements in both three-body and two-body decays

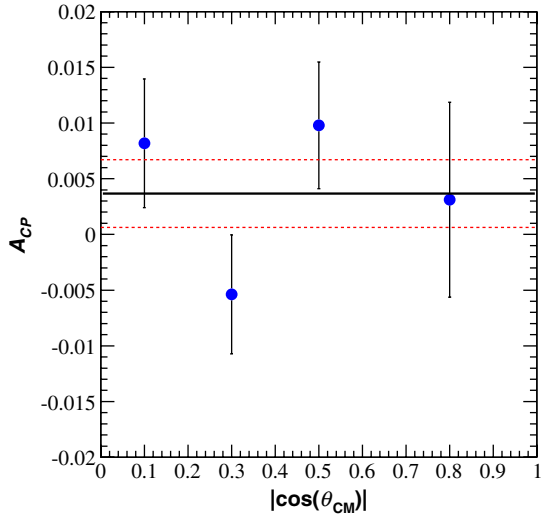

FIG. 2 (color online). *CP* asymmetry as a function of $|\cos(\theta_{CM})|$. The solid line represents the central value of A_{CP} and the dashed lines the ± 1 standard deviation statistical uncertainty, determined from a χ^2 fit to a constant value.

[22–24]. The weighted average of values obtained using Eq. (4) is $A_{CP} = (0.37 \pm 0.30 \pm 0.15)\%$, where the uncertainties are statistical and systematic, respectively, with a probability of 21% that the asymmetries are null in all four intervals (Fig. 2).

VI. D^+ MASS FIT

The $K^+K^-\pi^+$ mass distribution is fitted with a double-Gaussian function with a common mean and a linear background (Fig. 3), plus a function describing radiative decays $D^+ \to K^+K^-\pi^+\gamma$. The PDF for radiative decays is obtained from the reconstructed mass distribution of $K^+K^-\pi^+\gamma$ events selected at the generator level in our MC additionally convolved with a Gaussian of width 2.26 MeV/c^2 and accounts for 1.5% of the signal. The fit to data gives a D^+ mass value of 1869.70 $\pm$ 0.01 MeV/c^2, where the uncertainty is statistical only. The signal region is defined to lie within $\pm 2\sigma_{D^+}$ of the peak, where $\sigma_{D^+} = \sqrt{f_1\sigma_1^2 + (1-f_1)\sigma_2^2}$ is 5.04 MeV/c^2, and contains a total of 227874 events; $\sigma_1(\sigma_2)$ is the standard deviation of the first (second) Gaussian component and $f_1 = 0.63$ is the fraction of the signal in the first Gaussian component. Separate fits to the $K^+K^-\pi^+$ and $K^+K^-\pi^-$ distributions yield $N_{D^+} = 113037 \pm 469$ and $N_{D^-} = 110663 \pm 467$ events, respectively. The ratio of efficiency-corrected yields (N/ϵ) is $R \equiv \frac{N_{D^+}/\epsilon_{D^+}}{N_{D^-}/\epsilon_{D^-}} = 1.020 \pm 0.006$. This ratio is used to account for remaining asymmetries that arise from physics- or detector-related processes, such as an insufficiently accurate simulation of the FB asymmetry or a residual detector asymmetry. Also, it is a less accurate measure of the asymmetry when the efficiency varies significantly as a function of $\cos(\theta_{CM})$, as for our experiment.

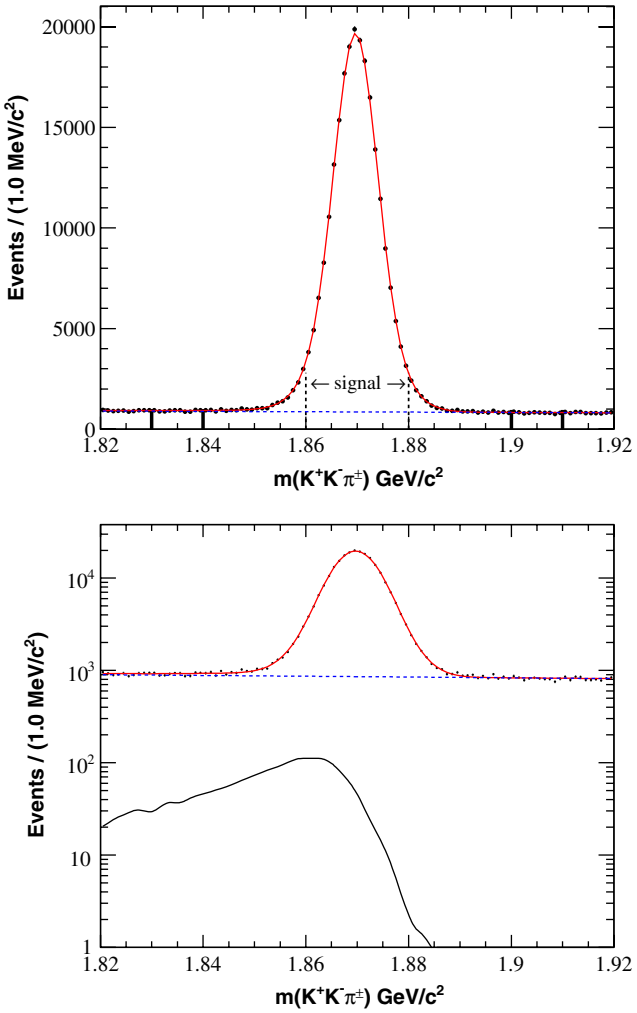

FIG. 3 (color online). Combined reconstructed invariant mass distribution $m(K^+K^-\pi^\pm)$ and projection of the fit result. The points show the data, the solid curve the fit model, and the dashed curve shows the background PDF. The signal region is indicated by the dashed vertical lines, and the sideband regions by the solid vertical lines. The lower figure shows the fit on a logarithmic scale with the radiative component of the signal PDF shown separately as a smooth curve.

VII. MODEL-INDEPENDENT SEARCHES FOR *CP* VIOLATION IN THE DALITZ PLOTS

Model-independent techniques to search for *CP* violation in the Dalitz plots are presented in Ref. [22]. The techniques include a comparison of the moment distributions and the asymmetry in the D^+ and D^- yields in various regions of the Dalitz plot. We scale the D^- yields by the factor R described in Sec. VI. By applying this correction, we remove residual detector-induced asymmetries and decouple, as far as possible, the search for *CPV* in the Dalitz plot from the search for *CPV* integrated over the phase space, which was described in Sec. V. We measure the *CP* asymmetry in the four regions of the Dalitz plot labeled A, B, C, and D in Fig. 4. We report the fitted yields,

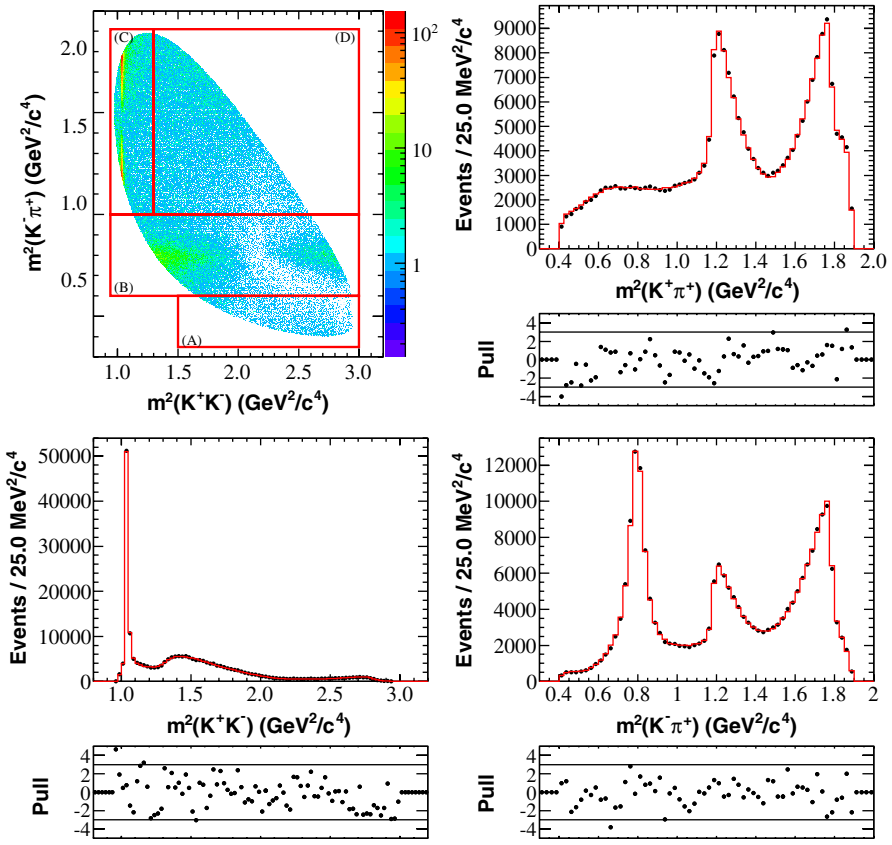

FIG. 4 (color online). $D^{\pm} \to K^+K^-\pi^{\pm}$ Dalitz plot and fit projections assuming no *CPV*, with the regions used for model-independent comparisons indicated as boxes. The A/B boundary is at $m_{K\pi} = 0.6\ \mathrm{GeV}^2/c^4$, the B/C boundary at $m_{K\pi} = 1.0\ \mathrm{GeV}^2/c^4$, and the C/D boundary at $m_{KK} = 1.3\ \mathrm{GeV}^2/c^4$. In the fit projections, the data are represented by points with error bars and the fit results by the histograms. The normalized residuals below each projection, defined as $(N_{\mathrm{Data}} - N_{\mathrm{MC}})/\sqrt{N_{\mathrm{MC}}}$, lie between $\pm 5\sigma$. The horizontal lines correspond to $\pm 3\sigma$.

average Dalitz plot efficiencies, and *CP* asymmetries in Table I.

We pursue a second technique in search of *CPV*, by measuring normalized residuals Δ for the efficiency-corrected and background-subtracted D^+ and D^- Dalitz plots, where Δ is defined by

$$\Delta \equiv \frac{n(D^+) - Rn(D^-)}{\sqrt{\sigma^2(D^+) + R^2\sigma^2(D^-)}}, \tag{5}$$

with $n(D^+)$ and $n(D^-)$ the observed number of D^+ and D^- mesons in an interval of the Dalitz plot, where $\sigma(D^+)$ and $\sigma(D^-)$ are the corresponding statistical uncertainties. The results for Δ are shown in Fig. 5. Note that the intervals for Fig. 5 are adjusted so that each interval contains approximately the same number of events. We calculate the quantity $\chi^2/(\nu - 1) = (\sum_{i=1}^{\nu} \Delta^2)/(\nu - 1)$, where ν is the number of intervals in the Dalitz plot. We fit the distribution of normalized residuals to a Gaussian function, whose mean and root-mean-squared (rms) deviation values we find to be consistent with zero and one, respectively. We obtain $\chi^2 = 90.2$ for 100 intervals with a Gaussian residual mean of 0.08 ± 0.15, rms deviation of 1.11 ± 0.15, and a consistency at the 72% level that the Dalitz plots do not exhibit *CP* asymmetry.

TABLE I. Yields, efficiencies, and *CP* asymmetry in the regions of the Dalitz plot shown in Fig. 4. For the *CP* asymmetry, the first uncertainty is statistical and the second is systematic.

Dalitz plot region	$N(D^+)$	$\epsilon(D^+)[\%]$	$N(D^-)$	$\epsilon(D^-)[\%]$	$A_{CP}[\%]$
(A) Below $\bar{K}^*(892)^0$	1882 ± 70	7.00	1859 ± 90	6.97	$-0.7 \pm 1.6 \pm 1.7$
(B) $\bar{K}^*(892)^0$	36770 ± 251	7.53	36262 ± 257	7.53	$-0.3 \pm 0.4 \pm 0.2$
(C) $\phi(1020)$	48856 ± 289	8.57	48009 ± 289	8.54	$-0.3 \pm 0.3 \pm 0.5$
(D) Above $\bar{K}^*(892)^0$ and $\phi(1020)$	25616 ± 244	8.01	24560 ± 242	8.00	$1.1 \pm 0.5 \pm 0.3$

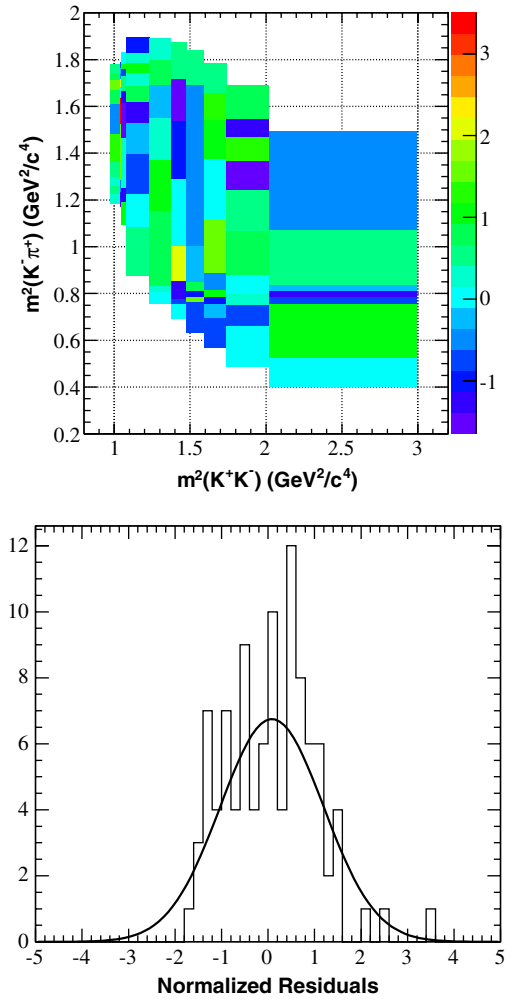

FIG. 5 (color online). Normalized residuals of the D^+ and D^- Dalitz plots in equally populated intervals (top) and their distribution fitted with a Gaussian function (bottom).

The Legendre polynomial moments of the cosine of the helicity angle of the $D^{\pm}$ decay products reflect the spin and mass of the intermediate resonant and nonresonant amplitudes and the interference effects among them [25]. A comparison of these moments between the D^+ and D^- two-body mass distributions provides a model-independent method to search for CP violation in the Dalitz plot and to study its mass and spin structure. We define the helicity angle θ_H for decays $D^+ \to (r \to K^+K^-)\pi^+$ via resonance r as the angle between the K^+ direction in the K^+K^- rest frame and the prior direction of the K^+K^- system in the D^+ rest frame. For decays $D^+ \to (r \to K^-\pi^+)K^+$ via resonance r, we define θ_H as the angle between the K^- direction in the $K^-\pi^+$ system and the prior direction of the $K^-\pi^+$ system in the D^+ rest frame.

The Legendre polynomial moment distribution for order l is defined as the efficiency-corrected and background-subtracted invariant two-body mass distribution $m(K^+K^-)$ or $m(K^-\pi^+)$, weighted by the spherical harmonic $Y_l^0[\cos(\theta_H)] = \sqrt{2l+1/4\pi}P_l[\cos(\theta_H)]$, where P_l is the Legendre polynomial. We define the two-body invariant mass interval weight $W_i^{(l)} \equiv (\sum_j w_{ij}^{(l)S} - \sum_k w_{ik}^{(l)B})/\langle\epsilon_i\rangle$, where $w_{ij}^{(l)}(w_{ik}^{(l)})$ is the value of Y_l for the jth (kth) event in the ith interval and $\langle\epsilon_i\rangle$ is the average efficiency for the ith interval. The superscripts S and B refer to the signal and background components, respectively. The uncertainty on $W_i^{(l)}$ is $\sigma^{(l)} \equiv \sqrt{\sum_j (w_{ij}^{(l)S})^2 + \sum_k (w_{ik}^{(l)B})^2/\langle\epsilon_i\rangle^2}$. To study differences between the D^+ and D^- amplitudes, we calculate the quantities X_i^l for l, ranging from zero to seven in a two-body invariant mass interval, where

$$X_i^l = \frac{(W_i^{(l)}(D^+) - RW_i^{(l)}(D^-))}{\sqrt{\sigma_i^{(l)^2}(D^+) + R^2\sigma_i^{(l)^2}(D^-)}}. \tag{6}$$

We calculate the χ^2/ndof over 36 mass intervals in the K^+K^- and $K^-\pi^+$ moments using

$$\chi^2 = \sum_i \sum_{l_1} \sum_{l_2} X_i^{(l_1)} \rho_i^{l_1 l_2} X_i^{(l_2)}, \tag{7}$$

where $\rho_i^{l_1 l_2}$ is the correlation coefficient between X^{l_1} and X^{l_2},

$$\rho_i^{l_1 l_2} \equiv \frac{\langle X_i^{(l_1)} X_i^{(l_2)}\rangle - \langle X_i^{(l_1)}\rangle\langle X_i^{(l_2)}\rangle}{\sqrt{\langle X_i^{(l_1)^2}\rangle - \langle X_i^{(l_1)}\rangle^2}\sqrt{\langle X_i^{(l_2)^2}\rangle - \langle X_i^{(l_2)}\rangle^2}}, \tag{8}$$

and where the number of degrees of freedom is given by the product of the number of mass intervals and the number of moments, minus one due to the constraint that the overall rates of D^+ and D^- mesons be equal. We find χ^2/ndof to be 1.10 and 1.09 for the K^+K^- and $K^-\pi^+$ moments, respectively (for ndof = 287), which corresponds to a probability of 11% and 13%, again respectively, for the null hypothesis (no CPV).

VIII. MODEL-DEPENDENT SEARCH FOR CP VIOLATION IN THE DALITZ PLOT

The Dalitz plot amplitude $\mathcal{A}$ can be described by an isobar model, which is parametrized as a coherent sum of amplitudes for a set of two-body intermediate states r. Each amplitude has a complex coefficient, i.e., $\mathcal{A}_r[m^2(K^+K^-), m^2(K^-\pi^+)] = \sum_r \mathcal{M}_r e^{i\phi_r} F_r[m^2(K^+K^-), m^2(K^-\pi^+)]$ [26–28], where $\mathcal{M}_r$ and ϕ_r are real numbers, and the F_r are dynamical functions describing the intermediate resonances. The complex coefficient may also be parameterized in Cartesian form, $x_r = \mathcal{M}_r \cos\phi_r$ and $y_r = \mathcal{M}_r \sin\phi_r$. We choose the $\bar{K}^*(892)^0$ as the reference amplitude in the CP-symmetric and CP-violating fits to the data, such that $\mathcal{M}_{\bar{K}^*(892)^0} = 1$ and $\phi_{\bar{K}^*(892)^0} = 0$.

Using events from the sideband regions (defined in Fig. 3) of the D^+ mass distribution, we model the CP conserving background, which is comprised of the $\bar{K}^*(892)^0$ and $\phi(1020)$ resonance contributions and combinatorial background. The combinatorial background

outside the resonant regions has a smooth shape and is modeled with the nonparametric k-nearest-neighbor density estimator [29]. The $\bar{K}^*(892)^0$ and $\phi(1020)$ regions are composed of the resonant structure and a linear combinatorial background, which we parametrize as a function of the two-body mass and the cosine of the helicity angle. The model consists of a Breit-Wigner (BW) PDF to describe the resonant line shape, and a first-order polynomial in mass to describe the combinatorial shape. These are further multiplied by a sum over low-order Legendre polynomials to model the angular dependence.

Assuming no *CPV*, we perform an unbinned maximum-likelihood fit to determine the relative fractions for the following resonances contributing to the decay: $\bar{K}^*(892)^0$, $\bar{K}^*(1430)^0$, $\phi(1020)$, $a_0(1450)$, $\phi(1680)$, $\bar{K}_2^*(1430)^0$, $\bar{K}^*(1680)^0$, $\bar{K}_1^*(1410)^0$, $f_2(1270)$, $f_0(1370)$, $f_0(1500)$, $f_2'(1525)$, $\kappa(800)$, $f_0(980)$, $f_0(1710)$, and a nonresonant (NR) constant amplitude over the entire Dalitz plot. We minimize the negative log likelihood function

$$-2\ln\mathcal{L} = -2\sum_{i=1}^{N}\ln\left[p(m_i)\frac{\epsilon_{\rm MC}(x_1,x_2)S(x_1,x_2)}{\int\int\epsilon_{\rm MC}(x_1,x_2)S(x_1,x_2)\mathrm{d}x_1\mathrm{d}x_2} + (1-p(m_i))\frac{B(x_1,x_2)}{\int\int B(x_1,x_2)\mathrm{d}x_1\mathrm{d}x_2}\right], \quad (9)$$

where N is the number of events. The reconstructed D^+ mass-dependent probability $p(m)$ is defined as $p(m_i) = \frac{S(m_i)}{S(m_i)+B(m_i)}$, where $S(m)$ and $B(m)$ are the signal and background PDFs, whose parameters are determined from the mass fit described in Sec. VI; $x_1 = m^2(K^+K^-)$ and $x_2 = m^2(K^-\pi^+)$, $S(x_1,x_2)$ is the Dalitz plot amplitude-squared, $\epsilon_{\rm MC}$ is the ANN efficiency, and $B(x_1,x_2)$ is the CP-symmetric background PDF.

The mass and width values of several resonances, including the $\bar{K}^*(892)^0$ and $\phi(1020)$, are determined in the fit (Table II). The $f_0(980)$ resonance is modeled with an effective BW parametrization,

$$A_{f_0(980)} = \frac{1}{m_0^2 - m^2 - im_0\Gamma_0\rho_{KK}}, \quad (10)$$

determined in the partial-wave analysis of $D_s^+ \to K^+K^-\pi^+$ decays [30], where $\rho_{KK} = 2p/m$ with p the momentum of the K^+ in the K^+K^- rest frame, $m_0 = 0.922$ GeV/c^2, and $\Gamma_0 = 0.24$ GeV. The remaining resonances (defined as $r \to AB$) are modeled as relativistic BWs,

$$\mathrm{RBW}(M_{AB}) = \frac{F_rF_D}{M_r^2 - M_{AB}^2 - i\Gamma_{AB}M_r}, \quad (11)$$

where Γ_{AB} is a function of the mass M_{AB}, the momentum p_{AB} of either daughter in the AB rest frame, the spin of the resonance, and the resonance width Γ_R. The form factors F_r and F_D model the underlying quark structure of the parent particle of the intermediate resonances. Our model for the $K^-\pi^+$ $\mathcal{S}$-wave term consists of the $\kappa(800)$, the $\bar{K}_0^*(1430)^0$, and a nonresonant amplitude. Different parametrizations for this term [31,32] do not provide a better description of data. The resulting fit fractions are summarized in Table III. We define a χ^2 value as

$$\chi^2 = \sum_i^{N_{\rm bins}}\frac{(N_i - N_{{\rm MC}_i})^2}{N_{{\rm MC}_i}}, \quad (12)$$

where $N_{\rm bins}$ denotes 2209 intervals of variable size. The ith interval contains N_i events (around 100), and $N_{{\rm MC}_i}$ denotes the integral of the Dalitz-plot model within the interval. We find $\chi^2/\mathrm{ndof} = 1.21$ for $\mathrm{ndof} = 2165$. The distribution of the data in the Dalitz plot, the projections of the data and the model of the Dalitz plot variables, and the one-dimensional residuals of the data and the model are shown in Fig. 4.

To allow for the possibility of *CPV* in the decay, resonances with a fit fraction of at least 1% (see Table III) are permitted to have different D^+ and D^- magnitudes and

TABLE II. Resonance mass and width values determined from the isobar model fit to the combined Dalitz-plot distribution.

Resonance	Mass (MeV/c^2)	Width (MeV)
$\bar{K}^*(892)^0$	895.53 ± 0.17	44.90 ± 0.30
$\phi(1020)$	1019.48 ± 0.01	4.37 ± 0.02
$a_0(1450)$	1441.59 ± 3.77	268.58 ± 5.28
$\bar{K}_0^*(1430)^0$	1431.88 ± 5.89	293.62 ± 3.83
$\bar{K}^*(1680)^0$	1716.88 ± 21.03	319.28 ± 109.07
$f_0(1370)$	1221.59 ± 2.46	281.48 ± 6.6
$\kappa(800)$	798.35 ± 1.79	405.25 ± 5.05

TABLE III. Fit fractions of the resonant and nonresonant amplitudes in the isobar model fit to the data. The uncertainties are statistical.

Resonance	Fraction (%)
$\bar{K}^*(892)^0$	21.15 ± 0.20
$\phi(1020)$	28.42 ± 0.13
$\bar{K}_0^*(1430)^0$	25.32 ± 2.24
NR	6.38 ± 1.82
$\kappa(800)$	7.08 ± 0.63
$a_0(1450)^0$	3.84 ± 0.69
$f_0(980)$	2.47 ± 0.30
$f_0(1370)$	1.17 ± 0.21
$\phi(1680)$	0.82 ± 0.12
$\bar{K}_1^*(1410)$	0.47 ± 0.37
$f_0(1500)$	0.36 ± 0.08
$a_2(1320)$	0.16 ± 0.03
$f_2(1270)$	0.13 ± 0.03
$\bar{K}_2^*(1430)$	0.06 ± 0.02
$\bar{K}^*(1680)$	0.05 ± 0.16
$f_0(1710)$	0.04 ± 0.03
$f_2'(1525)$	0.02 ± 0.01
Sum	97.92 ± 3.09

TABLE IV. *CP*-violating parameters from the simultaneous Dalitz plot fit. The first uncertainties are statistical and the second are systematic.

Resonance	$r_{CP}(\%)$	$\Delta\phi(^\circ)$
$\bar{K}^*(892)^0$	0. (FIXED)	0. (FIXED)
$\phi(1020)$	$0.35^{+0.82}_{-0.82} \pm 0.60$	$7.43^{+3.55}_{-3.50} \pm 2.35$
$\bar{K}_0^*(1430)^0$	$-9.40^{+5.65}_{-5.36} \pm 4.42$	$-6.11^{+3.29}_{-3.24} \pm 1.39$
NR	$-14.30^{+11.67}_{-12.57} \pm 5.98$	$-2.56^{+7.01}_{-6.17} \pm 8.91$
$\kappa(800)$	$2.00^{+5.09}_{-4.96} \pm 1.85$	$2.10^{+2.42}_{-2.45} \pm 1.01$
$a_0(1450)^0$	$5.07^{+6.86}_{-6.54} \pm 9.39$	$4.00^{+4.04}_{-3.96} \pm 3.83$
	Δx	Δy
$f_0(980)$	$-0.199^{+0.106}_{-0.110} \pm 0.084$	$-0.231^{+0.100}_{-0.105} \pm 0.079$
$f_0(1370)$	$0.019^{+0.049}_{-0.048} \pm 0.022$	$-0.0045^{+0.037}_{-0.039} \pm 0.016$

phase angles in the decay amplitudes ($\mathcal{A}$ or $\bar{\mathcal{A}}$). We perform a simultaneous fit to the D^+ and D^- data, where we parametrize each resonance with four parameters: $\mathcal{M}_r$, ϕ_r, r_{CP}, and $\Delta\phi_{CP}$. The *CP*-violating parameters are $r_{CP} = \frac{|\mathcal{M}_r|^2 - |\bar{\mathcal{M}}_r|^2}{|\mathcal{M}_r|^2 + |\bar{\mathcal{M}}_r|^2}$ and $\Delta\phi_{CP} = \phi_r - \bar{\phi}_r$. In the case of $\mathcal{S}$-wave resonances in the K^+K^- system, which make only small contributions to the model, we use instead the Cartesian form of the *CP* parameters, Δx and Δy, to parametrize the amplitudes and asymmetries. This choice of parametrization removes or eliminates technical problems with the fit. For these resonances we therefore introduce the parameters $x_r(D^\pm) = x_r \pm \Delta x_r/2$ and $y_r(D^\pm) = y_r \pm \Delta y_r/2$. The masses and widths determined in the initial fit (shown in Table II) are fixed, while the remaining parameters are determined in the fit. In Table IV, we report the *CP* asymmetries, i.e., either the polar-form pair (r_{CP}, $\Delta\phi_{CP}$) or the Cartesian pair (Δx_r, Δy_r). Figure 6 shows the difference between the Dalitz-plot projections of the D^+ and D^- decays, for both the data and the fit, where we weight the D^- events by the quantity R described in Sec. VI. It is evident from the figure that both the charge asymmetry of the data and fit are consistent with zero and with each other.

IX. SYSTEMATIC UNCERTAINTIES

We consider the following sources of systematic uncertainty: the $R_{\mathcal{L}}$ selection, corrections applied to the MC, binning of the data in $\cos(\theta_{\rm CM})$, and the Dalitz plot model.

To evaluate the uncertainty due to the $R_{\mathcal{L}}$ selection, we vary the selection such that the yield varies by at least ± 1 standard deviation and assign a systematic uncertainty defined by the largest variation with respect to the nominal value of the *CP* asymmetry.

The uncertainty due to corrections of the production model in the simulation (described in Sec. IV) is evaluated by randomly sampling the correction factors from a Gaussian distribution using their central values and uncertainties as the mean and sigma, respectively. The efficiency is then reevaluated and the fit is reperformed, floating the *CP* parameters while keeping other parameters fixed. This entire procedure is repeated 50 times. We take the rms deviation of the 50 fit values of the *CP* parameters to obtain the systematic uncertainty estimate. The uncertainty due to the tracking asymmetry correction is evaluated by comparing the measurement with two different corrections, namely the "Tau31" correction and the correction used in our analysis of $D^+ \to K^0_S\pi^+$ decays [24]. The average tracking asymmetry in the latter analysis is $(0.23 \pm 0.05)\%$, which is consistent with the result presented in Sec. IV after accounting for the different momentum spectra. We take the difference between the *CP* asymmetry central values using the two different tracking asymmetry corrections as the systematic uncertainty.

The integrated measurement results from binning the data in $\cos(\theta_{\rm CM})$. To evaluate the effect of the binning in $\cos(\theta_{\rm CM})$ for the integrated *CP* measurement, we vary the number of intervals and the interval edges and measure the *CP* asymmetry as the average asymmetry from a single forward interval and a single backward interval. Systematic uncertainties are determined from the difference between the nominal central value and the value determined from the alternative methods. We report these uncertainties for the integrated measurement in Table V.

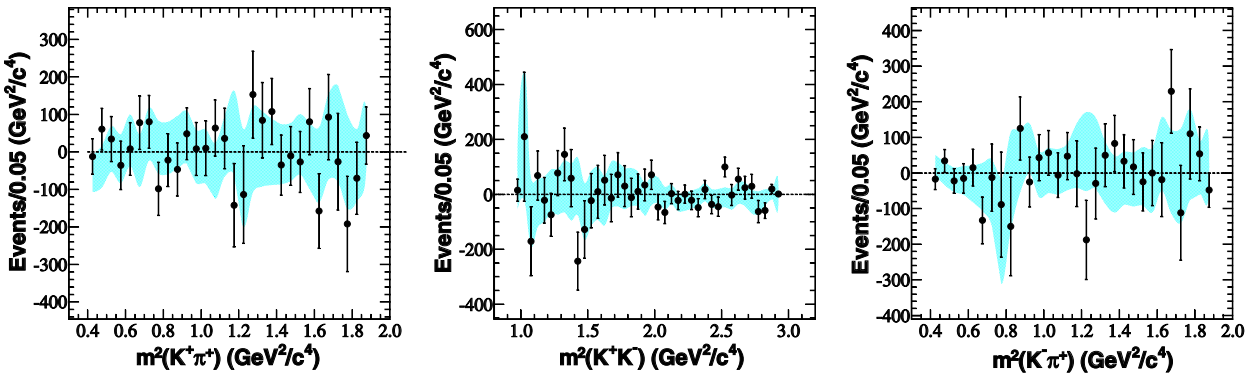

FIG. 6 (color online). The difference between the D^+ and D^- Dalitz plot projections of data (points) and of the fit (cyan band). The width of the band represents the ± 1 standard deviation statistical uncertainty expected for the size of our data sample.

TABLE V. Systematic uncertainties for the integrated CP asymmetry.

Average $\cos(\theta)$ asymmetry	$\Delta A_{CP}[\%]$
Event selection	0.07
Single forward and backward bin	0.01
$\cos(\theta_{\rm CM})$ binning	0.04
Track asymmetry correction	0.12

These systematic uncertainties are combined in quadrature to obtain the final result.

To determine the model-dependent uncertainty on the Dalitz-plot CPV parameters, we remove resonances with fit fractions less than 1%, one resonance at a time, and repeat the fit. We change the standard value of the radius parameter in the Blatt-Weisskopf form factor [28] for the intermediate resonance decay vertex from 1.5 GeV^{-1} to 1.0 GeV^{-1}. We take the maximum variation as the model-dependent systematic uncertainty. Systematic uncertainties for the Dalitz-plot-fit CPV parameters are listed in Table IV.

Finally, we study possible systematic effects on the binned Dalitz-plot results presented in Sec. VII. The nominal probability for the null CPV hypothesis is 72% for 100 intervals, while it is 42%, 62%, and 73%, respectively, for 25, 49, and 144 intervals. In comparison, changing the $\text{R}_{\mathcal{L}}$ selection, as described above, changes the nominal probability to 81%.

X. SUMMARY

In summary, we do not find any evidence for CP violation in the SCS decay $D^+ \to K^+K^-\pi^+$. The integrated CP asymmetry obtained using Eq. (4) is $(0.37 \pm 0.30 \pm 0.15)\%$. We find that the asymmetries in four regions of the Dalitz plot are consistent with zero, as listed in Table I. In addition, the D^+ and D^- Dalitz plots are consistent with no CP asymmetry with a probability of 72%, according to the analysis of the normalized residuals for the D^+ and D^- Dalitz plot divided into 100 equally populated intervals. Finally, we find no evidence for CP asymmetry in decays through various intermediate states from a study of the two-body mass distributions, as seen in Fig. 6, and from a parametrization of the Dalitz plot for which the CP asymmetries in amplitudes are listed in Table IV.

ACKNOWLEDGMENTS

We are grateful for the extraordinary contributions of our PEP-II colleagues in achieving the excellent luminosity and machine conditions that have made this work possible. The success of this project also relies critically on the expertise and dedication of the computing organizations that support *BABAR*. The collaborating institutions wish to thank SLAC for its support and the kind hospitality extended to them. This work is supported by the U.S. Department of Energy and the National Science Foundation, the Natural Sciences and Engineering Research Council (Canada), the Commissariat à l'Energie Atomique and Institut National de Physique Nucléaire et de Physique des Particules (France), the Bundesministerium für Bildung und Forschung and Deutsche Forschungsgemeinschaft (Germany), the Istituto Nazionale di Fisica Nucleare (Italy), the Foundation for Fundamental Research on Matter (The Netherlands), the Research Council of Norway, the Ministry of Education and Science of the Russian Federation, Ministerio de Ciencia e Innovación (Spain), and the Science and Technology Facilities Council (United Kingdom). Individuals have received support from the Marie-Curie IEF program (European Union), the A. P. Sloan Foundation (USA), and the Binational Science Foundation (USA-Israel).

[1] N. Cabibbo, Phys. Rev. Lett. **10**, 531 (1963); M. Kobayashi and T. Maskawa, Prog. Theor. Phys. **49**, 652 (1973).
[2] B. Bhattacharya, M. Gronau, and J. L. Rosner, Phys. Rev. D **85**, 054014 (2012).
[3] H. Y. Cheng and C. W. Chiang, Phys. Rev. D **85**, 034036 (2012).
[4] Y. Grossman, A. L. Kagan, and Y. Nir, Phys. Rev. D **75**, 036008 (2007).
[5] M. Artuso, B. Meadows, and A. A. Petrov, Annu. Rev. Nucl. Part. Sci. **58**, 249 (2008).
[6] R. Aaij *et al.* (LHCb Collaboration), Phys. Rev. Lett. **108**, 111602 (2012).
[7] T. Aaltonen *et al.* (CDF Collaboration), Phys. Rev. D **85**, 012009 (2012); Phys. Rev. Lett. **109**, 111801 (2012).
[8] Y. Grossman, A. L. Kagan, and J. Zupan, Phys. Rev. D **85**, 114036 (2012).
[9] G. F. Giudice, G. Isidori, and P. Paradisi, J. High Energy Phys. 4 (2012) 060.
[10] E. Franco, S. Mishima, and L. Silvestrini, J. High Energy Phys. 5 (2012) 140.
[11] All references in this paper to an explicit decay mode imply the use of the charge conjugate decay also, unless otherwise specified.
[12] P. Rubin *et al.* (CLEO Collaboration), Phys. Rev. D **78**, 072003 (2008).
[13] R. Aaij *et al.* (LHCb Collaboration), Phys. Rev. D **84**, 112008 (2011).
[14] B. Aubert *et al.* (*BABAR* Collaboration), Nucl. Instrum. Methods Phys. Res., Sect. A **479**, 1

(2002); W. Menges, IEEE Nucl. Sci. Symp. Conf. Rec. **5**, 1470 (2006).
[15] T. Sjöstrand, Comput. Phys. Commun. **82**, 74 (1994).
[16] S. Agostinelli *et al.* (Geant4 Collaboration), Nucl. Instrum. Methods Phys. Res., Sect. A **506**, 250 (2003).
[17] P. Golonka and Z. Was, Eur. Phys. J. C **45**, 97 (2006).
[18] A. Ryd, D. Lange, N. Kuznetsova, S. Versille, M. Rotondo, D. P. Kirkby, F. K. Wuerthwein, and A. Ishikawa, Report No. EVTGEN-V00-11-07.
[19] K. Nakamura *et al.* (Particle Data Group), J. Phys. G **37**, 075021 (2010).
[20] J. Schwindling, B. Mansoulie, MLPfit v1.40, http://schwind.home.cern.ch/schwind/MLPfit.html
[21] T. Allmendinger *et al.*, Nucl. Instrum. Methods Phys. Res., Sect. A **704**, 44 (2013).
[22] B. Aubert *et al.* (*BABAR* Collaboration), Phys. Rev. D **78**, 051102(R) (2008).
[23] B. Aubert *et al.* (*BABAR* Collaboration), Phys. Rev. Lett. **100**, 061803 (2008).
[24] P. del Amo Sanchez *et al.* (*BABAR* Collaboration), Phys. Rev. D **83**, 071103(R) (2011).
[25] B. Aubert *et al.* (*BABAR* Collaboration), Phys. Rev. D **76**, 011102(R) (2007).
[26] S. Kopp *et al.* (CLEO Collaboration), Phys. Rev. D **63**, 092001 (2001).
[27] D. Asner, arXiv:hep-ex/0410014.
[28] J. Blatt and V. Weisskopf, *Theoretical Nuclear Physics* (Wiley, New York, 1952).
[29] R. O. Duda and P. E. Hart, *Pattern Classification and Scene Analysis* (Wiley, New York, 1973).
[30] P. del Amo Sanchez *et al.* (*BABAR* Collaboration), Phys. Rev. D **83**, 052001 (2011).
[31] P. del Amo Sanchez *et al.* (*BABAR* Collaboration), Phys. Rev. Lett. **105**, 081803 (2010).
[32] E. M. Aitala *et al.* (E791 Collaboration), Phys. Rev. D **73**, 032004 (2006); **74**, 059901(E) (2006).